Physical interaction of junctophilin and the $Ca_V1.1$C-terminus is crucial for skeletal muscle contraction

Tsutomu Nakada[a,1], Toshihide Kashihara[a], Masatoshi Komatsu[a,b], Katsuhiko Kojima[c], Toshikazu Takeshita[c], and Mitsuhiko Yamada[a,1]

[a]Department of Molecular Pharmacology, Shinshu University School of Medicine, Matsumoto, Nagano, Japan; [b]Department of Orthopaedic Surgery, Shinshu University School of Medicine, Matsumoto, Nagano, Japan; [c]Department of Microbiology and Immunology, Shinshu University School of Medicine, Matsumoto, Nagano, Japan

Short title: JP and $Ca_V1.1$ interaction for muscle contraction

[1]Correspondence to:
Mitsuhiko Yamada, MD, Ph.D. (orcid.org/0000-0002-7515-3824)
3-1-1 Asahi, Matsumoto, Nagano 390-8621 Japan
FAX: +81-263-37-3085
TEL: +81-263-37-2605
E-mail: myamada@shinshu-u.ac.jp
or
Tsutomu Nakada, Ph.D. (orcid.org/0000-0002-7662-6742)
3-1-1 Asahi, Matsumoto, Nagano 390-8621 Japan
FAX: +81-263-37-3085
TEL: +81-263-37-2606
E-mail: tnakada@shinshu-u.ac.jp

Abstract

Close physical association of $Ca_V1.1$ L-type calcium channels (LTCCs) at the sarcolemmal junctional membrane (JM) with ryanodine receptors (RyRs) of the sarcoplasmic reticulum (SR) is crucial for excitation–contraction coupling (ECC) in skeletal muscle. However, the molecular mechanism underlying the JM targeting of LTCCs is unexplored. Junctophilins (JPs) 1 and 2 stabilize the JM by bridging the sarcolemmal and SR membranes. Here we examined the roles of JPs in localization and function of LTCCs. Knockdown of JP1 or 2 in cultured myotubes inhibited LTCC clustering at the JM and suppressed evoked Ca^{2+} transients without disrupting JM structure. Coimmunoprecipitation and glutathione S-transferase (GST) pull-down assays demonstrated that JPs physically interacted with 12 amino acid residues in the proximal C-terminus of the $Ca_V1.1$. A JP1 mutant lacking the C-terminus including the transmembrane domain (JP1ΔCT) interacted with the sarcolemmal/T-tubule membrane but not the SR membrane. Expression of this mutant in adult mouse muscles *in vivo* exerted a dominant-negative effect on endogenous JPs, impairing LTCC–RyR coupling at triads without disrupting JM morphology, and substantially reducing Ca^{2+} transients without affecting SR Ca^{2+} content. Moreover, the contractile force of the JP1ΔCT-expressed muscle was dramatically reduced compared with the control. Taken together, JPs recruit LTCCs to the JM through physical interaction and ensure robust ECC at triads in skeletal muscle.

Significance Statement

For robust contraction of skeletal muscles, the L-type calcium channel acts as a key molecule by transducing membrane depolarization to calcium release from the sarcoplasmic reticulum.

Proper intracellular localization of L-type calcium channels at the junctional membrane complex where the plasma membranes are closely apposed to the membranes of the sarcoplasmic reticulum is necessary for this process. Junctophilins are known to stabilize the structure of the junctional membrane complex by bridging the plasma membrane and the sarcoplasmic membrane. We report for the first time that junctophilins recruit L-type calcium channels to the junctional membrane through physical interaction with the $Ca_V1.1$ subunits of the channels. This protein–protein interaction at triads ensures efficient contraction in differentiated adult skeletal muscle.

\body

Introduction

L-type calcium channels (LTCCs) play a central role in excitation–contraction coupling (ECC) of skeletal muscle (1). The skeletal muscle LTCC is composed of pore-forming $Ca_V1.1$ and ancillary β_1, $\alpha_2\delta$, and γ subunits (2). The voltage-sensitive domain of $Ca_V1.1$ detects action potentials traversing the muscle fiber membrane (sarcolemma) and opens ryanodine receptors (RyRs) in the adjacent sarcoplasmic reticulum (SR) through its II-III loop and β_1 subunits to release Ca^{2+} into the cytoplasm (3). In skeletal muscle, LTCCs and RyRs are clustered at triad junctions where invaginations of the sarcolemmal membrane called transverse tubules (T-tubules) are closely juxtaposed to two terminal cisternae of the SR (4, 5). Association of a single cistern of the SR with T-tubules or plasma membrane, called a diad or peripheral coupling, respectively, is also present in several types of excitable cells, including cardiac myocytes. These membrane structures are collectively referred to as junctional membrane (JM) complexes. Although the proper localization of LTCCs *vis¬à¬vis* RyRs at triads is essential for ECC in striated muscles, the molecular mechanism of this targeting is still elusive.

Myotubes of $Ca_V1.1$-deficient dysgenic (*mdg*) mice are a valuable tool to investigate the function and localization of LTCCs in muscle (6-10). Using myotubes differentiated from the immortalized dysgenic myoblast cell line GLT, we and others have identified the motifs necessary for the JM targeting of LTCCs in the C-terminus of $Ca_V1.1$ and cardiac $Ca_V1.2$ subunits (8, 10). However, it is still unknown how these motifs recruit LTCCs to the JM.

Junctophilins (JPs) are molecules that stabilize the JM complex by bridging the sarcolemmal and SR membranes via their N-terminal lipid-binding membrane occupation

and recognition nexus (MORN) motif and C-terminal transmembrane domain, respectively (11). Four members of the JP family (JP1–4) have been identified in the mammalian genome. JP1 is expressed in skeletal muscle, JP2 in skeletal and cardiac muscle (11), and JP3 and 4 in the brain (12). Golini et al. demonstrated that JPs physically interact with both LTCCs and RyRs in skeletal muscle (13). This report also showed that transfection of a siRNA against JPs disrupted the normal punctate distributions of LTCCs and RyRs indicative of JM localization in C2C12 myotubes. In cardiac myocytes, JP2 physically interacts with the LTCC $Ca_V1.2$ subunit and modulates the Ca^{2+} current (14). Thus, in addition to bridging the sarcolemmal and SR membranes, JPs may physically interact with LTCCs and thereby directly support LTCC–RyR coupling in cultured striated muscle.

In this study, we first confirmed that JPs support LTCC–RyR coupling and ECC in cultured myotubes. Biochemical analyses demonstrated that JPs physically interact with the proximal C-termini of $Ca_V1.1$ subunits and that disruption of this interaction dislocates LTCCs out of the JM. Then, we transduced a JP1 mutant lacking its C-terminus including transmembrane domain (JP1ΔCT) in adult mouse tibialis anterior (TA) and flexor digitorum brevis (FDB) muscles using adeno-associated virus (AAV) vectors. This mutant was previously shown to interact with the sarcolemmal membrane but not the SR membrane (11). Interestingly, JP1ΔCT targeted LTCCs over the entire sarcolemma, disturbed LTCC–RyR coupling in triads, and significantly reduced evoked Ca^{2+} transients and the contractile force of muscles without disrupting the triad structure or reducing SR Ca^{2+} content. Thus, we provide compelling evidence that JPs recruit LTCCs to precise locations at triads through physical interaction and ensure robust ECC in adult skeletal muscle.

Results

Inhibition of LTCC and RyR junctional membrane targeting by JP knockdown. JPs are localized to the JM in skeletal myocytes and myotubes (11, 15). We performed immunocytochemistry on myotubes differentiated from a $Ca_V1.1$-lacking GLT cell line to confirm colocalization of JPs, LTCCs, and RyRs. In these GLT-derived myotubes, transduced green fluorescent protein (GFP)-$Ca_V1.1$ and endogenous RyR, JP1, and JP2 showed punctate colocalization, indicating that they all accumulated at the JM (Fig. S1A). We then introduced a siRNA against JP1 and/or JP2 into GLT-derived myotubes to assess the role of JPs in the JM targeting of LTCCs and RyRs. Western blotting showed that all three tested siRNAs against either JP1 or JP2 effectively and selectively suppressed expression of JP1 or JP2 (Fig. S1B). We used JP1 siRNA #2 and JP2 siRNA #1 for subsequent experiments. Immunocytochemistry also showed the effectiveness and selectivity of these siRNAs in GLT-derived myotubes (Figs. S1C and D). It is noteworthy that JP1 knockdown did not inhibit JP2 clustering and *vice versa*, indicating that either JP1 or JP2 alone can form JM complexes and that knockdown of either alone does not disrupt the JM.

Nevertheless, transfection of a siRNA against JP1 or JP2 significantly inhibited the JM targeting of GFP-$Ca_V1.1$ in GLT myotubes (Figs. 1A and B). Junctional membrane targeting of endogenous $Ca_V1.1$ was also suppressed in C2C12 myotubes by knockdown of JP1 or JP2 (Figs. S2A and B). These results suggest that in addition to creating the JM, JP1, and JP2 may function to directly recruit plasma membrane LTCCs. In contrast, the JM targeting of RyRs was inhibited by JP2 but not by JP1 siRNA in both GLT and C2C12 myotubes (Figs. 1 and S2), suggesting that JM localization of RyRs is determined solely by JP2. Cotransfection of siRNA-resistant JP1 or JP2 constructs rescued the inhibition of the JM targeting of $Ca_V1.1$ and RyRs (Fig. S2C).

Effect of JP knockdown on ECC in myotubes. The effect of JP knockdown on LTCC ionic and gating currents in C2C12 myotubes was examined. Knockdown of JP2 but not JP1

significantly reduced LTCC ionic currents (Figs. 2A and B). However, expression of $Ca_V1.1$ protein was not affected by transfection of siRNAs against JPs (Fig. 2C). Moreover, neither JP1 nor JP2 siRNA affected gating currents (Figs. 2D and E), indicating that JPs did not affect the membrane expression of LTCCs.

Nevertheless, knockdown of JP1 or JP2 significantly reduced the number of C2C12 myotubes exhibiting twitch Ca^{2+} transients in response to field stimulation (Fig. 2F). Moreover, the peak amplitude of Ca^{2+} transients in responding cells was also significantly reduced by JP1 or JP2 siRNA (Figs. 2G and H). However, these siRNAs did not affect cyclopiazonic acid (CPA)-induced Ca^{2+} release from the SR (Figs. 2I and J), indicating that knockdown of JPs did not affect the SR Ca^{2+} content. These results indicate that JP1 and JP2 siRNAs may inhibit the efficient coupling of LTCCs and RyRs.

Physical interaction of JPs with the proximal C-terminus of $Ca_V1.1$. A physical interaction of JPs with LTCCs and RyRs was previously reported (14, 16). We confirmed this interaction by a coimmunoprecipitation assay using mouse skeletal muscle microsomes (Fig. 3A). We henceforth focused on the molecular mechanism and physiological significance of the interaction between LTCCs and JPs. We first performed a glutathione S-transferase (GST) pull-down assay to identify the JP-binding motif of the LTCC. The cytoplasmic N-terminus, I-II loop, II-III loop, III-IV loop, proximal C-terminus, and distal C-terminus of $Ca_V1.1$ were purified as GST-fused recombinant proteins using a bacterial expression system. The result showed that the proximal C-terminus (PCT) binds to JP1 and JP2 (Fig. 3B). To narrow down the binding motif, we constructed several recombinant proteins bearing different PCT fragments and repeated the GST pull-down assay (Fig. 3C). Unfortunately, the region between fragments #2 and #3 could not be examined because the corresponding protein could not be solubilized under any conditions we tested (Fig. 3C). Through these experiments, however, we could narrow down the JP-binding motif (JBM) to a stretch of 12 amino acid

residues (i.e., #11, amino acids 1595–1606) (Fig. 3C).

Contribution of the JBM of $Ca_V1.1$ to JM targeting. We compared the amino acid sequence of the JBM of $Ca_V1.1$ with that of the corresponding regions of cardiac $Ca_V1.2$ and neuronal $Ca_V2.1$ subunits across different species (Fig. 4A). Multiple alignments indicated that the amino acid sequence of the JBM was well conserved in $Ca_V1.1$ and cardiac $Ca_V1.2$, but a similar sequence was not present anywhere in neuronal $Ca_V2.1$. We purified these regions of $Ca_V1.2$ and $Ca_V2.1$ as GST-proteins, and once again performed the pull-down assay. As expected, recombinant $Ca_V1.1$ and $Ca_V1.2$, but not $Ca_V2.1$, bound to JPs (Fig. 4C).

To identify the crucial amino acid residues in the JBM, we conducted alanine scanning and performed a GST pull-down assay (Fig. S3A). This experiment revealed that the binding capacities of I1597A, R1599A, R1600A, L1604A, and F1605A mutants were clearly lower than that of the wild type (Fig. 4B). We introduced three representative mutations, R1596A, which caused partial inhibition, and R1600A and R1605A, which caused total inhibition, into the full-length $Ca_V1.1$ and expressed them in GLT myotubes. Immunocytochemical analysis showed that the R1600A and R1605A mutations, but not the R1596A mutation, significantly decreased the JM targeting of $Ca_V1.1$ compared with the wild type (Figs. 4D and S3B). Expression of the channel proteins and gating charge movement were not significantly different between wild type and R1600A-transfected myotubes, indicating that the mutant normally localized in plasma membranes (Figs. 4E, F, and G). Expression of R1600A did not affect the JM targeting of JP1, JP2, and RyR (Fig. S3C). In contrast, the Ca^{2+} transients in response to field stimulation were significantly reduced in R1600A-transfected myotubes compared with wild type controls (Figs 4H, I, and J). These results suggest that physical binding of $Ca_V1.1$ to JPs is necessary for LTCC–RyR coupling and ECC.

Physiological outcome of *in vivo* overexpression of a C-terminus-deleted JP1 mutant in

differentiated muscles of living mice. Takeshima et al. showed that a C-terminus including a transmembrane domain-deleted mutant of JP1 diffusely localized to the plasma membrane of *Xenopus* oocytes and Madin–Darby canine kidney cells, indicating that the mutant can interact with the sarcolemmal membrane but not the SR membrane (11). We prepared a similar C-terminus-deleted mutant of JP1 with 3xFLAG tag in the C-terminus (JP1ΔCT-FLAG). Note that JP1ΔCT-FLAG lacking the C-terminal epitope was not recognized by the anti-JP1 antibody used in this study. This is advantageous, because endogenous JP1 and exogenous JP1ΔCT-FLAG can be separately identified with anti-JP1 and anti-FLAG antibodies, respectively (Fig. S3D).

In GLT myotubes, transiently expressed JP1ΔCT-FLAG was not specifically clustered to the JM but was diffusely localized over the entire plasma membrane (Fig. 5A). In the same myotubes, the JM targeting of coexpressed GFP-$Ca_V1.1$ was significantly inhibited (Fig. 5A), indicating that JP1ΔCT-FLAG lacks the capacity to guide GFP-$Ca_V1.1$ to the JM. On the contrary, JM localization of LTCCs was not affected by expression of a negative control FLAG-PLCδPH, an unrelated protein also known to diffusely localize to the entire plasma membrane (Fig. 5A). Protein expression and membrane localization of $Ca_V1.1$ were not affected by JP1ΔCT-FLAG transfection (Figs. 5B, C, and D). JM targeting of JP1, JP2, and RyR was also not affected by JP1ΔCT-FLAG expression (Fig. S3E). These results suggest that JP1ΔCT-FLAG elicits a dominant-negative effect on the JM targeting of LTCCs and can be utilized as a tool to disrupt LTCC–RyR coupling in living muscles.

Therefore, we constructed an AAV vector carrying JP1ΔCT-FLAG. Twenty days after direct intramuscular injection of the virus into the flexor digitorum brevis (FDB) muscle of mice, expression of JP1ΔCT-FLAG was observed in >80% of isolated fibers (Fig. S4A). Immunocytochemical analysis revealed that JP1ΔCT-FLAG was equally distributed in T-tubule and sarcolemmal membranes in the low-level expression fibers (~30% of positive

fibers). In the major population of JP1ΔCT-FLAG-expressed fibers, the mutant was more strongly localized to the sarcolemmal membrane than the T-tubule membrane (~70% of positive fibers) (Figs. 5E and S4B). Interestingly, abundant LTCC signals were observed in the sarcolemma of JP1ΔCT-FLAG-expressing fibers, but not in control fibers (Figs. 5E and S4C). The localizations of JP1, JP2, and RyRs were not altered by JP1ΔCT-FLAG expression (Fig. S4D). Although the results clearly indicated that JP1ΔCT-FLAG changed LTCC localization, a considerable amount of LTCC signals still remained in the T-tubules. In contrast to myotubes, punctate distribution of $Ca_V1.1$ was not detected in the T-tubules of adult FDB fibers by our immunocytochemical analysis. Therefore, we performed a proximity ligation assay (PLA) to reveal whether JP1ΔCT disturbed the coupling of LTCCs with JPs and RyRs in whole cells, including sarcolemma and T-tubules. PLA is a technique that detects an interaction of two molecules *in situ* using specific antibodies and probes labeled by short DNA strands. PLA revealed that exogenous JP1ΔCT-FLAG strongly interacted with $Ca_V1.1$, whereas a much weaker interaction between JP1ΔCT-FLAG and RyRs was observed (Fig. S4E). The PLA assay also revealed that interactions between $Ca_V1.1$ and RyRs were significantly inhibited by JP1ΔCT-FLAG (Fig. 5F). Inhibition of physical interaction between $Ca_V1.1$ and JPs by JP1ΔCT-FLAG was also confirmed (Figs. 5G and S4E). Because JPs and RyRs were much more abundantly expressed in triads than in peripheral coupling (Fig. S4D), these results strongly suggest that JP1ΔCT-FLAG blocked interaction between $Ca_V1.1$ and JPs and thereby the coupling between $Ca_V1.1$ and RyRs at triads. Interactions of RyRs with JPs were not affected by JP1ΔCT-FLAG expression (Figs. 5G and S4E). In addition, a significant decrease in the peak amplitude of Ca^{2+} transients during tetanus was evident in JP1ΔCT-FLAG-expressing fibers (Fig. 5H). However, there was no difference in Ca^{2+} release from the SR induced by the Ca^{2+} releasing cocktail ICE (ionomycin, cyclopiazonic acid, EGTA) between control and JP1ΔCT-FLAG-expressing FDB fibers (Fig.

5H), indicating that JP1ΔCT-FLAG did not alter SR Ca^{2+} content. Thus, these data suggest that JP1ΔCT-FLAG inhibits ECC by disrupting the interaction of $Ca_V1.1$ with JPs and RyRs in triads.

Finally, we examined the impact of JP1ΔCT-FLAG overexpression on the contraction of TA muscle *in situ*. Expression of JP1ΔCT-FLAG was observed in almost all fibers in TA muscles by immunohistochemistry (Fig. S4F). Consistent with the PLA study using FDB fibers, reductions in physical interactions of $Ca_V1.1$ and JPs were observed by coimmunoprecipitation (Fig. 5I). No significant difference in cross-sectional area was observed between control and JP1ΔCT-FLAG-AAV-injected muscles (Fig. S4G), and transmission electron microscopic analysis revealed that JP1ΔCT-FLAG did not affect the distance between T-tubule membranes and SR membranes (Figs. S4H and I), indicating that JP1ΔCT-FLAG did not destroy the JM structure. However, JP1ΔCT-FLAG-AAV significantly decreased the contractile force of muscle at all stimulation frequencies between 1 and 200 Hz (Fig. 5J). These results provide compelling evidence that the precise localization of LTCCs in the JM by JPs and LTCC–RyR coupling at triads is crucial for efficient contraction of skeletal muscle.

Discussion

In this study, we show that knockdown of JP1 or 2 in myotubes inhibits the clustering of LTCCs in the JM and suppresses electrically evoked Ca^{2+} transients without disrupting JM structure. JPs physically interacted with the proximal C-terminus of $Ca_V1.1$, and disruption of this interaction by mutagenesis inhibited the JM clustering of LTCCs.

Because mice lacking JP1 die shortly after birth and JP2 knockouts die *in utero* (11, 17), it was impossible to analyze the functional significance of skeletal muscle JPs in adulthood with conventional knockout mice. In the present study, we therefore adopted a

novel approach to acutely transduce JP1ΔCT-FLAG-AAV in adult FDB and TA. Fortunately, the approach was not lethal and did not destroy the JM or reduce the SR Ca^{2+} content, but it selectively disrupted LTCC–RyR coupling at triads and inhibited ECC (Fig. 5). Immunoprecipitation and PLA indicated that JP1ΔCT-FLAG reduced $Ca_V1.1$–JP and $Ca_V1.1$–RyR interactions to ~30% (Figs. 5F and I). Because JPs and RyRs were much more abundantly expressed in triads than in peripheral coupling (Fig. S4D), these results strongly suggest that JP1ΔCT-FLAG blocked interaction between $Ca_V1.1$ and JPs and thereby the coupling between $Ca_V1.1$ and RyRs at triads. In the JM of skeletal muscle, four $Ca_V1.1$ channel molecules are arranged in orthogonal arrays called tetrads that correspond in position to the RyRs. The tetrad formation is critical for skeletal muscle-specific links between LTCCs and RyRs (18). One possibility is therefore that JP1ΔCT-FLAG hampered tetrad formation in triads by inhibiting the interaction between $Ca_V1.1$ and JPs. The detailed mechanism of action awaits further analysis; however, it was clear that inhibition of physical interaction of $Ca_V1.1$ and JPs by JP1ΔCT (Fig. 5I) leads to prominent defects in ECC. Thus, we provide compelling evidence that in addition to generating the JM complex, JPs function to directly recruit LTCCs to the JM through protein–protein interaction and support efficient physiological LTCC–RyR coupling in triads.

This effect of JPs is not simply due to suppression of $Ca_V1.1$ membrane expression. In fact, suppression of JP1 and/or JP2 did not change the gating charge of LTCCs in C2C12 myotubes (Fig. 2), indicating that JPs are not essential for membrane targeting of LTCCs. In contrast to our study, Golini et al. reported that JP1 and 2 siRNAs suppressed the expression and gating charge currents of LTCCs (13). Whereas the siRNAs were transfected at the myotube stage (2 days after differentiation started) in our study, they transfected them at the myoblast stage. It is possible that JPs are also necessary at an early stage of differentiation of the myotubes, and this may have caused a decrease in $Ca_V1.1$ expression in

the previous study.

JP1ΔCT-FLAG suppressed the interaction of LTCCs and JP1 as well as JP2 (Fig. 5I). Since the JBM in $Ca_V1.1$ can interact with both JP1 and 2, it is possible that JP1ΔCT-FLAG simultaneously inhibited the binding of both JPs to $Ca_V1.1$. Although both JP1 and JP2 are necessary for the JM targeting of LTCCs in skeletal muscle, there are functional differences between them. For instance, suppression of JP2, but not JP1, disturbed the JM targeting of RyRs in C2C12 myotubes (Fig. 1). Therefore, JP2 knockdown may more severely decouple $Ca_V1.1$ and RyR. RyR transmits a retrograde stimulatory signaling to $Ca_V1.1$ through this coupling (19), which may explain why JP2 but not JP1 siRNA significantly decreased LTCC ionic currents in the C2C12 myotubes (Fig. 2). However, it is proposed that JP2 may contribute to the creation of diads and peripheral couplings, while JP1 may contribute to the maturation of diads to triads during skeletal muscle differentiation. Therefore, JP1ΔCT inhibited ECC mainly by disrupting LTCC-JP1 coupling in triads.

To date, there have been several reports analyzing the Ca_V1 domain responsible for JM targeting. Flucher et al. determined that a 55-amino-acid sequence in the C-terminus (a.a. 1607–1661) contained the JM targeting signal of $Ca_V1.1$ (8). Nakada et al. reported that amino acid residues 1677–1708 in the C-terminus of cardiac $Ca_V1.2$ (corresponding to a.a. 1551–1583 of $Ca_V1.1$) were necessary for JM targeting (10). However, the JBM determined in this study (a.a. 1595–1606) does not exactly match these JM targeting signals, although it is located immediately proximal to Flucher's site and immediately distal to Nakada's site. It was shown that loss of Flucher's site led to a complete abolition of $Ca_V1.1$ JM targeting (8), indicating that this site is also necessary for JM targeting, in addition to our JBM. Thus, the JM targeting of $Ca_V1.1$ in skeletal muscle may be regulated by multiple sites and processes. Additional studies are necessary to identify what signal(s) are sufficient for the JM targeting of $Ca_V1.1$ in skeletal muscle.

To summarize, we have demonstrated that JP1 and JP2 can physically interact with the cytoplasmic C-terminus of the LTCC $Ca_V1.1$ subunit. In addition to guiding the formation of JM complexes, JPs localize LTCCs to the JM and enable the channels to efficiently couple with RyRs at triads through this protein–protein interaction. This mechanism is crucial for efficient ECC in differentiated adult skeletal muscle.

Materials and Methods

The detailed materials and methods are described in *SI Materials and Methods.*

Animals. All experimental procedures were conducted in accordance with the Guidelines for Animal Experimentation of Shinshu University and approved by the Committee for Animal Experimentation. Isolation of skeletal muscles and AAV injection were performed using 10- to 13-week-old male C57BL/6 mice.

Cell culture. C2C12 and GLT myoblast cell lines were differentiated to myotubes in low serum condition.

Molecular cloning and AAV production. All plasmid vectors were produced by standard molecular biology techniques. For preparation of AAV vectors, the AAVpro Helper Free system (Clontech, Mountain View, CA, USA) was used according to the manufacturer's protocols.

Immunocytochemistry, immunohistochemistry, and PLA. Immunocytochemistry and immunohistochemistry were carried out by standard protocols. PLA was performed with Duolink systems (Sigma-Aldrich). All antibodies used in this study are listed in Table S1.

Patch clamp analysis. Ionic and gating currents of the LTCC were recorded in the whole-cell configuration at room temperature. Ca^+ imaging was conducted with Fluo-4/AM (Dojindo).

Measurement of contractile forces. The contractile forces of TA muscles were measured *in vivo* according to the methods described in a previous study with minor modification (20).

GST-fusion protein production and pull-down assay. GST-fusion proteins were produced by a bacterial expression system using BL21 cells.

Preparation of microsomes. Gluteus and hindlimb muscles were dissected from mice, and microsomes were prepared. The resulting microsomes were solubilized in lysis buffer and used for western blotting, immunoprecipitation, and GST pull-down assay.

Immunoprecipitation and western blotting. Immunoprecipitation and western blotting were conducted as previously described, with minor modifications (21). All antibodies used in this study are listed in Table S1.

Statistical analysis. Data are shown as means ± SEM. Statistical significance was evaluated by Student's unpaired *t*-test. For multiple comparisons, analysis of variance with Bonferroni's test was used. A p-value < 0.05 was considered to indicate statistical significance.

Acknowledgments

We are grateful to Prof. Bernhard Flucher (Innsbruck Medical University), Prof. Manfred Grabner (Innsbruck Medical University), and Prof. William Catterall (University of Washington) for kindly providing the cDNA of α_1 subunits. We are grateful to Reiko Sakai for secretarial assistance. This work was supported by Grants-in-aid for Scientific Research 24590271 and 16K08491 from the Ministry of Education, Culture, Sport, Science and Technology of Japan (MEXT) and by The Novartis Foundation (Japan) for the Promotion of Science to T.N.

During the preparation of this manuscript, Perni et al. reported that $Ca_V1.1$, β_{1a}, Stac3, RyR1, and JP2 are sufficient to reproduce the skeletal muscle type ECC in tsA201 cells (22).

Author contributions: T.N., T.K., M.K., and K.K. collected and analyzed the data. T.N., T.T.,

and M.Y. contributed to the experimental design. T.N. and M.Y. prepared the manuscript.

The authors declare they have no conflicts of interest.

References

1. Calderón JC, Bolaños P, Caputo C (2014) The excitation-contraction coupling mechanism in skeletal muscle. *Biophys Rev* 6(1):133–160.

2. Arikkath J, Campbell KP (2003) Auxiliary subunits: essential components of the voltage-gated calcium channel complex. *Curr Opin Neurobiol* 13(3):298–307.

3. Tanabe T, Beam KG, Adams BA, Niidome T, Numa S (1990) Regions of the skeletal muscle dihydropyridine receptor critical for excitation-contraction coupling. *Nature* 346(6284):567–569.

4. Flucher BE, Morton ME, Froehner SC, Daniels MP (1990) Localization of the α_1 and α_2 subunits of the dihydropyridine receptor and ankyrin in skeletal muscle triads. *Neuron* 5(3):339–351.

5. Jorgensen AO, Shen AC, Arnold W, Leung AT, Campbell KP (1989) Subcellular distribution of the 1,4-dihydropyridine receptor in rabbit skeletal muscle in situ: an immunofluorescence and immunocolloidal gold-labeling study. *J Cell Biol* 109(1):135–147.

6. Powell JA, Petherbridge L, Flucher BE (1996) Formation of triads without the dihydropyridine receptor alpha subunits in cell lines from dysgenic skeletal muscle. *J Cell Biol* 134(2):375–387.

7. Neuhuber B, et al. (1998) Association of calcium channel α_{1S} and β_{1a} subunits is required for the targeting ofβ_{1a} but not of α_{1S} into skeletal muscle triads. *Proc Natl Acad Sci USA* 95(9):5015–5020.

8. Flucher BE, Kasielke N, Grabner M (2000) The triad targeting signal of the skeletal muscle calcium channel is localized in the COOH terminus of the alpha(1S) subunit. *J Cell Biol* 151(2):467–478.

9. Obermair GJ, et al. (2005) The Ca2+ channel alpha2delta-1 subunit determines Ca2+ current kinetics in skeletal muscle but not targeting of alpha1S or excitation-contraction coupling. *J Biol Chem* 280(3):2229–2237.

10. Nakada T, et al. (2012) Proximal C-terminus of α1C subunits is necessary for junctional membrane-targeting of cardiac L-type calcium channels. *Biochem J* 448:221–231.

11. Takeshima H, Komazaki S, Nishi M, Iino M, Kangawa K (2000) Junctophilins: a novel family of junctional membrane complex proteins. *Mol Cell* 6(1):11–22.

12. Nishi M, Sakagami H, Komazaki S, Kondo H, Takeshima H (2003) Coexpression of junctophilin type 3 and type 4 in brain. *Brain Res Mol Brain Res* 118(1-2):102–110.

13. Golini L, et al. (2011) Junctophilin 1 and 2 proteins interact with the L-type Ca2+ channel dihydropyridine receptors (DHPRs) in skeletal muscle. *J Biol Chem* 286(51):43717–43725.

14. Jiang M, et al. (2016) JPH-2 interacts with Cai-handling proteins and ion channels in dyads: Contribution to premature ventricular contraction-induced cardiomyopathy. *Heart Rhythm* 13(3):743–752.

15. Barone V, Randazzo D, Del Re V, Sorrentino V, Rossi D (2015) Organization of junctional sarcoplasmic reticulum proteins in skeletal muscle fibers. *J Muscle Res Cell Motil* 36(6):501–515.

16. Murphy RM, et al. (2012) Ca2+-dependent Proteolysis of Junctophilin 1 and Junctophilin 2 in Skeletal and Cardiac Muscle. *J Physiol (Lond)* 591(3):719–729.

17. Ito K, et al. (2001) Deficiency of triad junction and contraction in mutant skeletal muscle lacking junctophilin type 1. *J Cell Biol* 154(5):1059–1067.

18. Protasi F, et al. (2002) Multiple regions of RyR1 mediate functional and structural interactions with alpha(1S)-dihydropyridine receptors in skeletal muscle. *Biophys J* 83(6):3230–3244.

19. Nakai J, et al. (1996) Enhanced dihydropyridine receptor channel activity in the presence of ryanodine receptor. *Nature* 380(6569):72–75.

20. Cosgrove BD, et al. (2014) Rejuvenation of the muscle stem cell population restores strength to injured aged muscles. *Nat Med* 20(3):255–264.

21. Kashihara T, Nakada T, Kojima K, Takeshita T, Yamada M (2017) Angiotensin II activates CaV 1.2 Ca(2+) channels through β-arrestin2 and casein kinase 2 in mouse immature cardiomyocytes. *J Physiol (Lond)* 595(13):4207–4225.

22. Perni S, Lavorato M, Beam KG (2017) De novo reconstitution reveals the proteins required for skeletal muscle voltage-induced Ca^{2+} release. *Proc Natl Acad Sci USA* 114(52):13822–13827.

Figure Legends

Fig. 1. Knockdown of JP1 and JP2 inhibits the JM targeting of $Ca_V1.1$ and RyR in myotubes. (A) Immunocytochemistry showing the effect of JP1 or JP2 siRNA on the JM targeting of $Ca_V1.1$ and RyR in GLT myotubes. Bar = 20 μm. (B and C) The numbers of $Ca_V1.1$ and RyR clusters were quantified in siRNA-transfected myotubes. Values are means ± SEM (20 myotubes from 4 dishes were analyzed for each group). $^{**}p < 0.01$ vs. negative control.

Fig. 2. Effects of JP1 or JP2 knockdown on LTCC currents, gating charges, and Ca^{2+} transients in C2C12 myotubes. (A) Representative traces of LTCC currents at different membrane potentials. (B) Peak current density–voltage relationships of LTCCs. Mean ± SEM (n = 6–7). * $p < 0.05$ vs. control. (C) $Ca_V1.1$ expression. (D) Representative traces of LTCC gating currents at different membrane potentials. (E) The gating charge density–voltage relationships of LTCCs in C2C12 myotubes. Mean ± SEM (n = 6–7). (F) Absolute number of C2C12 myotubes in chambers responding to field stimulation with Ca^{2+} transients. Mean ± SEM. Myotubes in 7 to 9 dishes (153 mm^2) were counted. ** $p < 0.01$. (G) Representative traces of Ca^{2+} transients induced by electrical twitch stimulation. (H) Peak amplitude of twitch Ca^{2+} transients. Mean ± SEM (n = 12–23). ** $p < 0.01$. (I) Representative traces of Ca^{2+} transients induced by CPA treatment. (E) Peak amplitude of Ca^{2+} transients induced by CPA. Mean ± SEM (n = 12–16).

Fig. 3. Proximal C-terminus of $Ca_V1.1$ interacts with JPs. (A) Coimmunoprecipitation of $Ca_V1.1$, RyR, JP1, and JP2 from solubilized proteins from mouse skeletal muscle microsomes. (B) Pull-down assay with the GST-fused proteins. The N-terminus (NT), I-II loop (I-II), II-III loop (II-III), III-IV loop, proximal C-terminus (PCT), and distal C-terminus (DCT) of $Ca_V1.1$ were purified as GST-fused proteins. Proteins were pulled down with the recombinant

proteins from mouse skeletal muscle microsomes. (C) Pull-down assay with the GST-fused proteins. A scheme of constructed recombinant proteins of the $Ca_V1.1$ C-terminus is shown. Bars indicate the regions purified as recombinant proteins. The number on the right side of each bar corresponds to the lane number of the gel image. EF, EF-hand; IVS6, the sixth transmembrane segment in domain IV; IQ, IQ-motif.

Fig. 4. The JP-binding motif is involved in the JM targeting of $Ca_V1.1$. (A) Alignment of partial amino acid sequences of $Ca_V1.1$, $Ca_V1.2$, and $Ca_V2.1$ C-termini. The conserved amino acid residues between $Ca_V1.1$ and $Ca_V1.2$ are highlighted in red. (B) Series of single-alanine-substituted mutants of the JP-binding motif were purified and used for pull-down assay. (C) The recombinant protein bearing the JP-binding motif of $Ca_V1.1$ and the corresponding motif of $Ca_V1.2$ and $Ca_V2.1$ were used for pull-down assay. (D) Effect of alanine substitution at the JP-binding motif on channel clustering in GLT myotubes. Mean ± SEM ($n = 20$). $^{**}p < 0.01$ compared with WT. (E) Expression of WT or R1600A $Ca_V1.1$ in GLT myotubes. (F) Representative traces of LTCC gating currents in GLT myotubes. (G) Gating charge density–voltage relationships of LTCCs in GLT myotubes. Mean ± SEM ($n = 5$). (H) Absolute number of myotubes in chambers responding to field stimulation with Ca^{2+} transients. Mean ± SEM. The myotubes in six dishes (153 mm^2) were counted for each group. ** $p < 0.01$. (I) Representative traces of Ca^{2+} transients induced by electrical twitch stimulation. (J) Peak amplitude of twitch Ca^{2+} transients. Mean ± SEM ($n = 14–22$). ** $p < 0.01$.

Fig. 5. Expression of JP1ΔCT-FLAG decreases the coupling of $Ca_V1.1$–RyR and the specific force of the tibialis anterior muscle in living mice. (A) GLT myotubes were cotransfected with GFP-$Ca_V1.1$ and PLCδPH-FLAG (negative control) or JP1ΔCT-FLAG. GFP-$Ca_V1.1$ and FLAG-tag were detected with antibodies against GFP and FLAG, respectively. Bar = 20 μm. The graph represents the number of $Ca_V1.1$ clusters in the

myotubes. Mean ± SEM (n = 20). **p < 0.01 vs. control. (B) Expression of $Ca_V1.1$ and PLCδPH-FLAG or JP1ΔCT-FLAG in GLT myotubes. (C) Representative traces of LTCC gating currents in GLT myotubes. (D) Gating charge density–voltage relationships of LTCCs in GLT myotubes. Mean ± SEM (n = 5). (E) Effect of JP1ΔCT-FLAG expression on localization of $Ca_V1.1$ in FDB fibers. $Ca_V1.1$ and JP1ΔCT-FLAG in isolated FDB fibers were detected with antibodies against $Ca_V1.1$ and FLAG, respectively. Bar = 20 μm. High-magnification images of an x–y plane and an x–z plane are shown in the lower left and lower right panels, respectively. The dotted lines in the x–y plane indicate the position at which the x–z image was constructed. Bar = 1 μm. (F) Representative images and quantification of $Ca_V1.1$–RyR association detected by PLA assay. The collapsed z-stack images of FDB fibers are shown. Bar = 20 μm. Graph: normalized PLA-positive area (40 fibers from four animals for each group were analyzed). **p < 0.01 compared with control. (G) Normalized PLA-positive area analyzed with various antibody combinations (40 fibers from four animals for each group were analyzed). (H) Ca^{2+} transients of isolated FDB fibers induced by electrical stimulation or Ca^{2+}-releasing cocktail treatment. Action potentials were elicited by electrical stimulation with 1-ms pulses of 50 V at 100 Hz. The SR Ca^{2+} content was assessed by applying the Ca^{2+} release cocktail (ICE). The peak fluorescence amplitudes of Ca^{2+} transients elicited by tetanic and ICE stimulation were quantified in 74 to 80 and 19 to 24 fibers from four animals, respectively. Mean ± SEM. ** p < 0.01. (I) Immunoprecipitation and immunoblotting of TA muscle proteins. The left panel represents immunoblotting using microsomes from control- and JP1ΔCT-expressed TA muscle. The right panel represents immunoblotting using proteins that coimmunoprecipitated with anti-$Ca_V1.1$ antibody. The graphs represent the amounts of coimmunoprecipitated JP1 and JP2 normalized by expression in microsomes (n = 4). AU, arbitrary unit. Mean ± SEM. ** p < 0.01. (J) Frequency-specific force relationship of TA muscles. Twenty days after injection

of control or JP1ΔCT-FLAG-AAV, muscle contractile force was assayed *in vivo*. The TA muscles were electrically stimulated with 1-ms pulses of predetermined supramaximal voltage at 1 to 200 Hz. Mean ± SEM ($n = 6$). * $p < 0.01$ vs. control.

Fig. 1

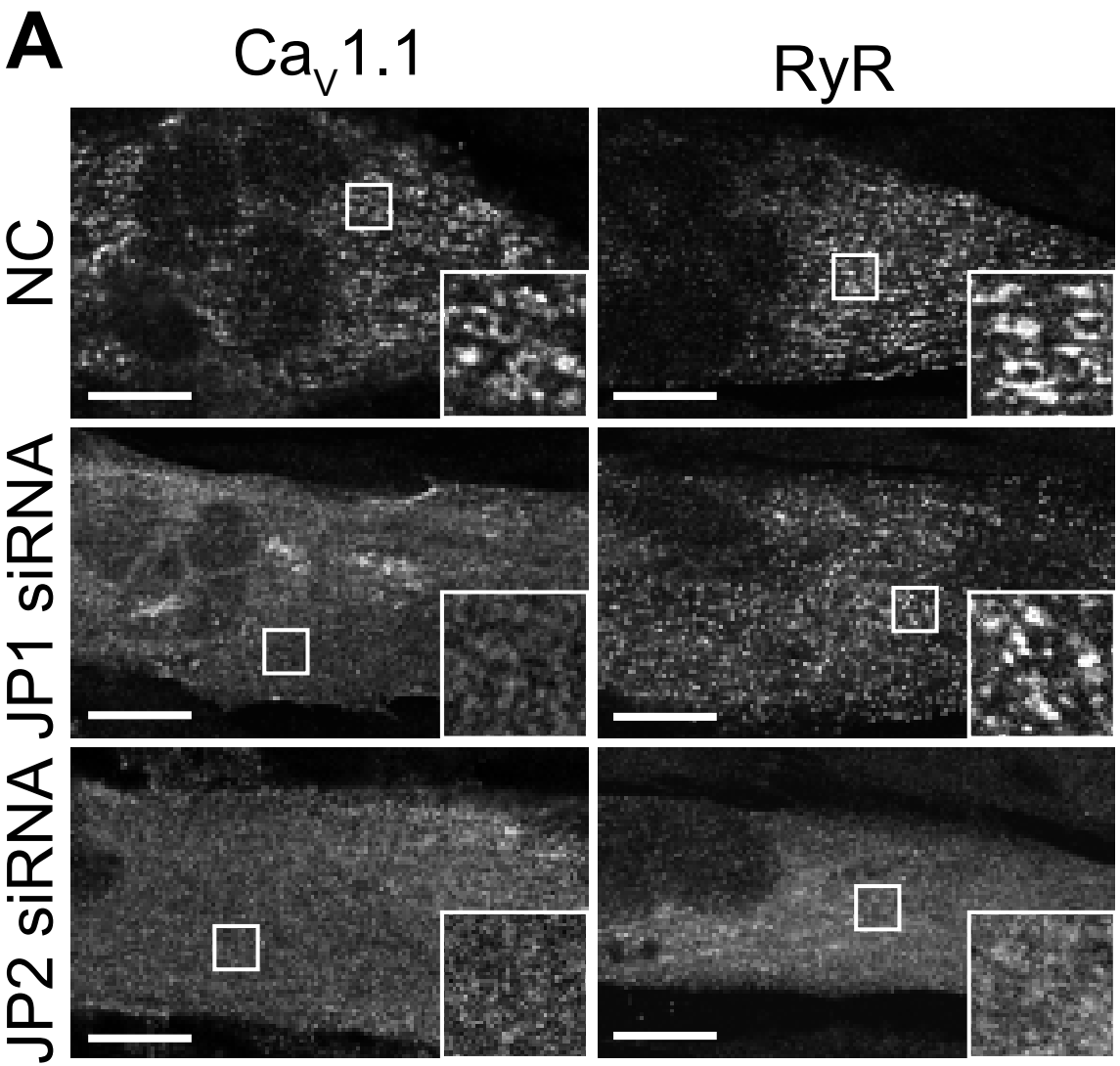
A
Ca$_V$1.1
RyR
NC
JP1 siRNA
JP2 siRNA

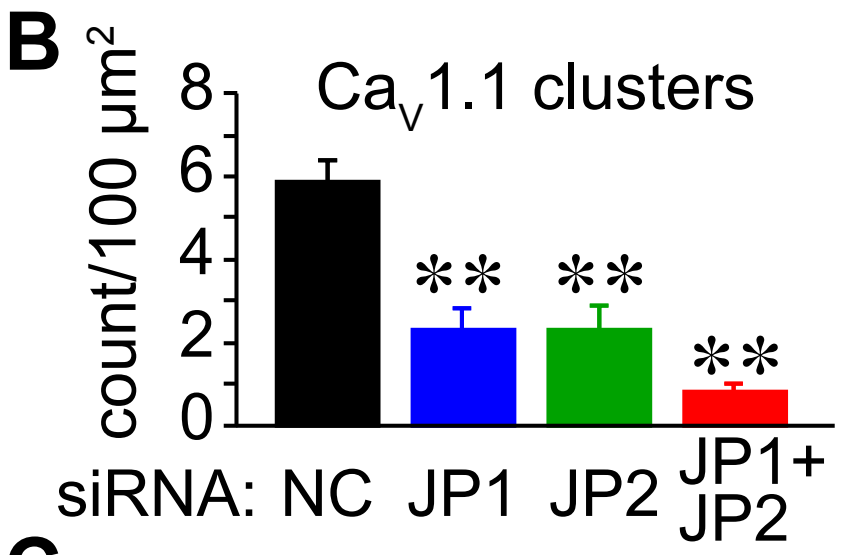
B
Ca$_V$1.1 clusters
count/100 μm^2
0
2
4
6
8
**
**
**
siRNA: NC JP1 JP2 JP1+ JP2

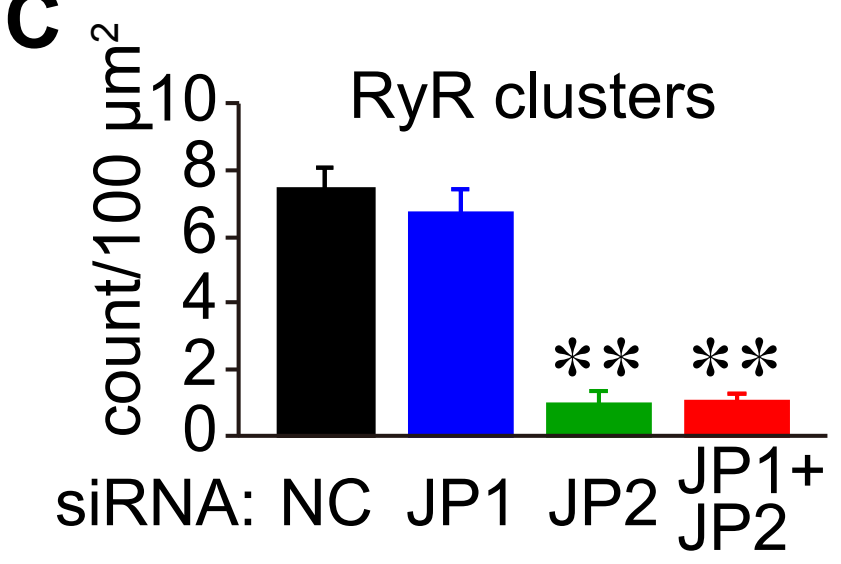
C
RyR clusters
count/100 μm^2
0
2
4
6
8
10
**
**
siRNA: NC JP1 JP2 JP1+ JP2

Fig. 2

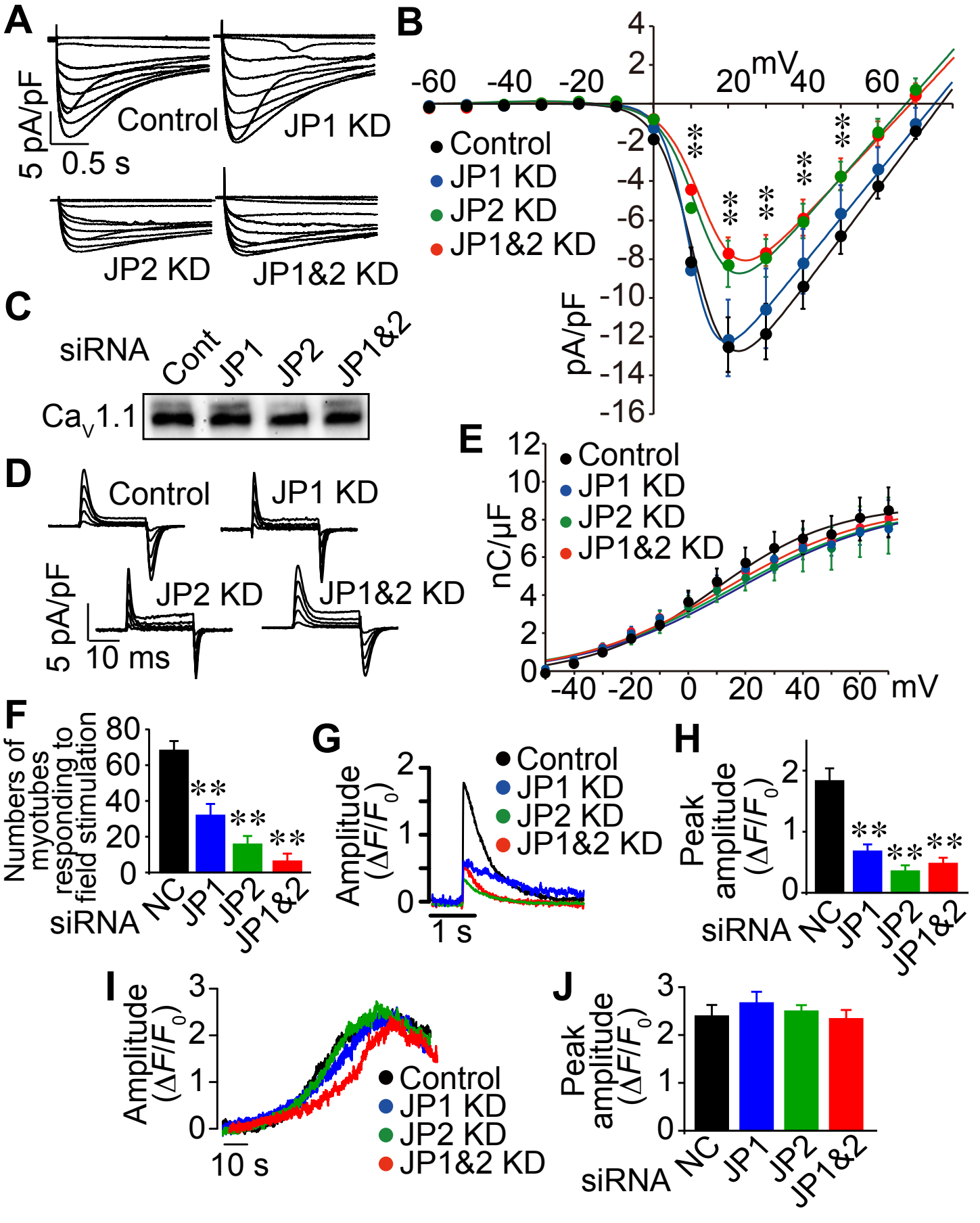
A
5 pA/pF
0.5 s
Control
JP1 KD
JP2 KD
JP1&2 KD
B
-60
-40
-20
20
mV
40
60
4
2
-2
-4
-6
-8
-10
-12
-14
-16
pA/pF
Control
JP1 KD
JP2 KD
JP1&2 KD
**
C
siRNA
Cont
JP1
JP2
JP1&2
Ca$_V$1.1
D
Control
JP1 KD
JP2 KD
JP1&2 KD
5 pA/pF
10 ms
E
12
10
8
6
4
2
0
nC/μF
Control
JP1 KD
JP2 KD
JP1&2 KD
-40
-20
0
20
40
60
mV
F
Numbers of myotubes responding to field stimulation
80
60
40
20
0
**
siRNA
NC
JP1
JP2
JP1&2
G
Amplitude ($\Delta F/F_0$)
2
1
0
Control
JP1 KD
JP2 KD
JP1&2 KD
1 s
H
Peak amplitude ($\Delta F/F_0$)
2
1
0
**
siRNA
NC
JP1
JP2
JP1&2
I
Amplitude ($\Delta F/F_0$)
3
2
1
0
10 s
Control
JP1 KD
JP2 KD
JP1&2 KD
J
Peak amplitude ($\Delta F/F_0$)
3
2
1
0
siRNA
NC
JP1
JP2
JP1&2

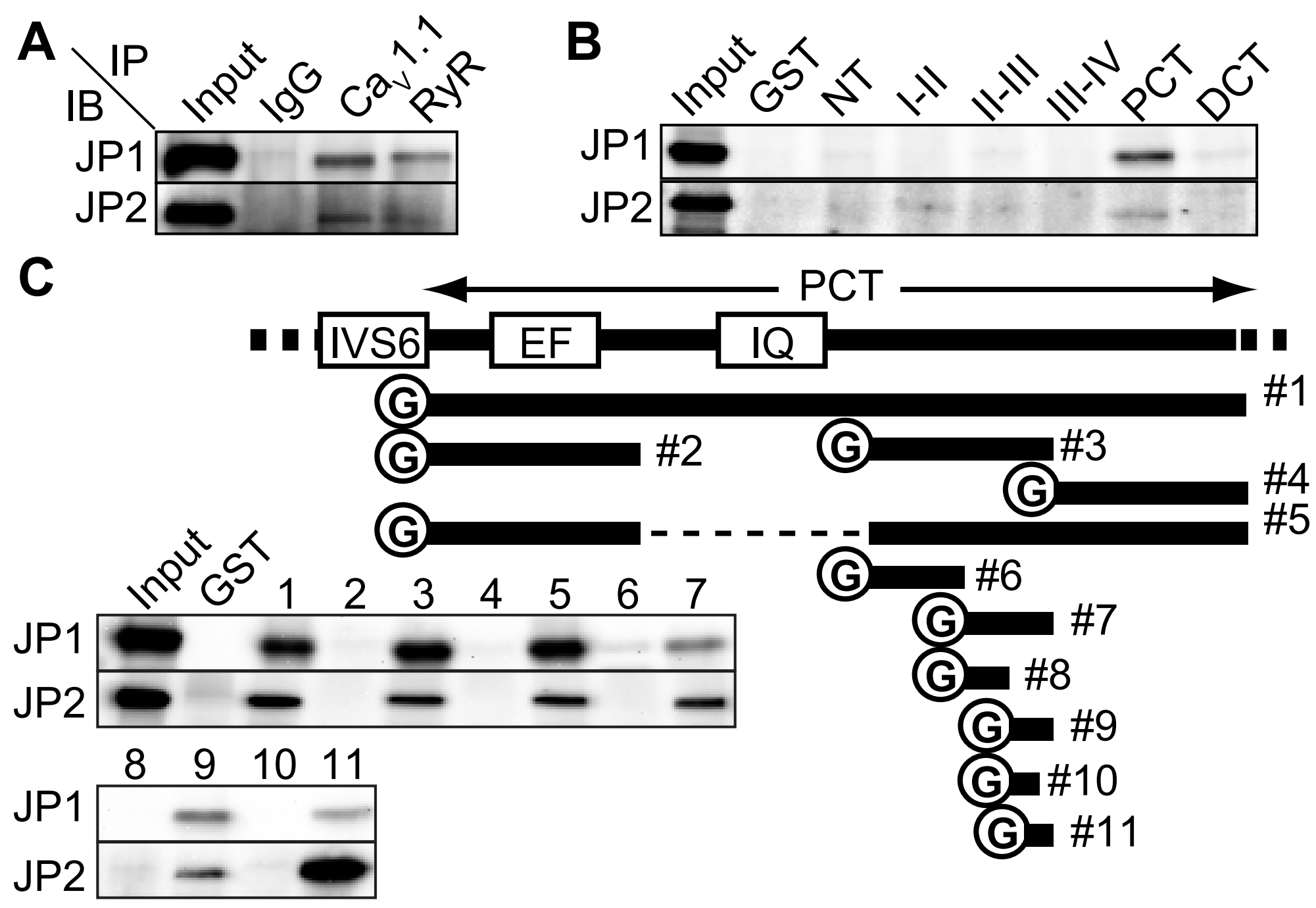
A
IP
IB
Input
IgG
Cav1.1
RyR
JP1
JP2
B
Input
GST
NT
I-II
II-III
III-IV
PCT
DCT
JP1
JP2
C
PCT
IVS6
EF
IQ
#1
#2
#3
#4
#5
#6
#7
#8
#9
#10
#11
Input
GST
1
2
3
4
5
6
7
JP1
JP2
8
9
10
11
JP1
JP2

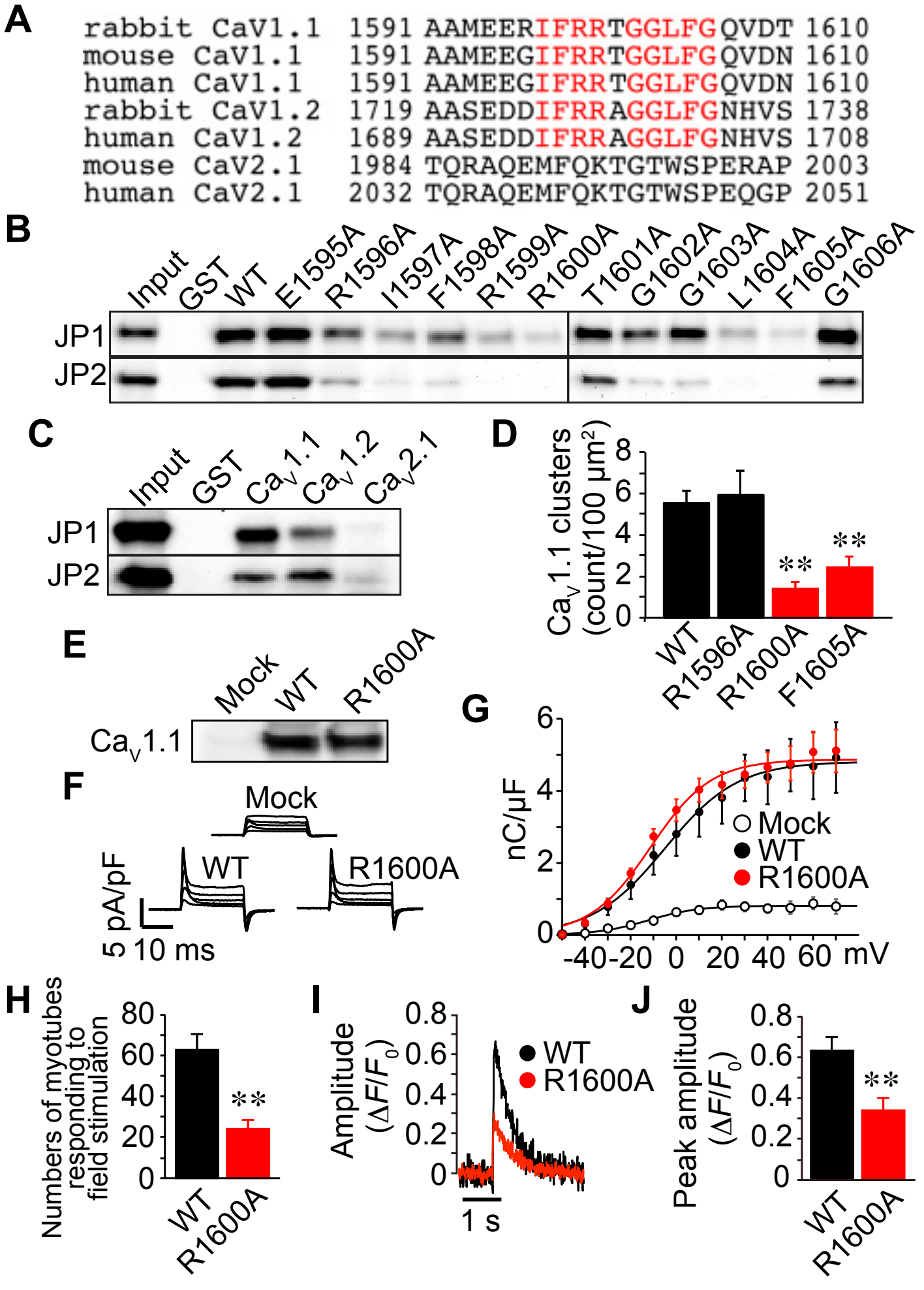
A
rabbit CaV1.1 1591 AAMEERIFRRTGGLFGQVDT 1610
mouse CaV1.1 1591 AAMEEGIFRRTGGLFGQVDN 1610
human CaV1.1 1591 AAMEEGIFRRTGGLFGQVDN 1610
rabbit CaV1.2 1719 AASEDDIFRRAGGLFGNHVS 1738
human CaV1.2 1689 AASEDDIFRRAGGLFGNHVS 1708
mouse CaV2.1 1984 TQRAQEMFQKTGTWSPERAP 2003
human CaV2.1 2032 TQRAQEMFQKTGTWSPEQGP 2051
B
Input
GST
WT
E1595A
R1596A
I1597A
F1598A
R1599A
R1600A
T1601A
G1602A
G1603A
L1604A
F1605A
G1606A
JP1
JP2
C
Input
GST
CaV1.1
CaV1.2
CaV2.1
JP1
JP2
D
CaV1.1 clusters (count/100 μm²)
0
2
4
6
8
**
**
WT
R1596A
R1600A
F1605A
E
Mock
WT
R1600A
CaV1.1
F
Mock
WT
R1600A
pA/pF
5
10 ms
G
nC/μF
0
2
4
6
Mock
WT
R1600A
-40 -20 0 20 40 60 mV
H
Numbers of myotubes responding to field stimulation
0
20
40
60
80
**
WT
R1600A
I
Amplitude (ΔF/F0)
0
0.2
0.4
0.6
0.8
WT
R1600A
1 s
J
Peak amplitude (ΔF/F0)
0
0.2
0.4
0.6
0.8
**
WT
R1600A

Fig. 5

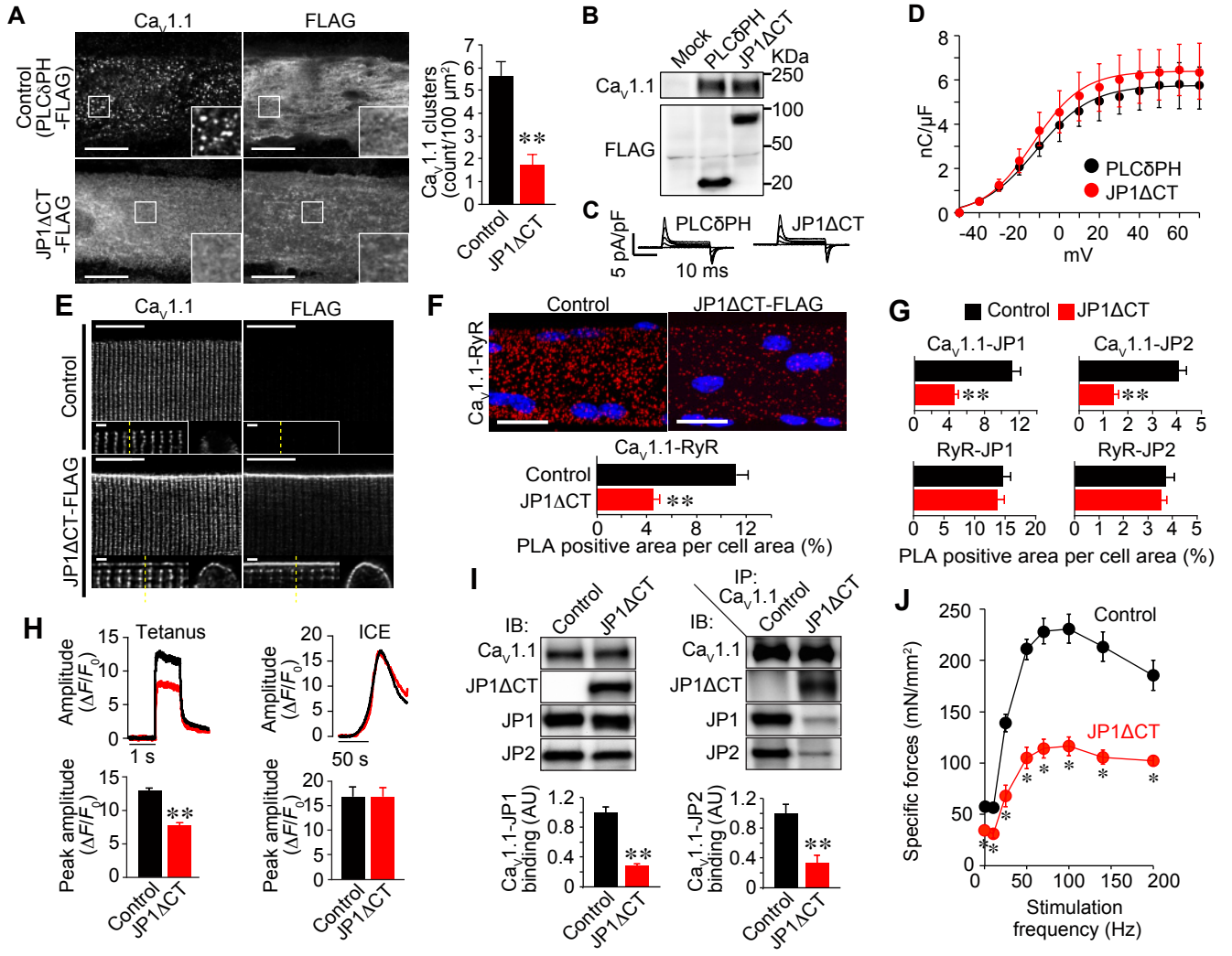
A
Ca$_V$1.1
FLAG
Control (PLCδPH -FLAG)
JP1ΔCT -FLAG
Ca$_V$1.1 clusters (count/100 μm^2)
Control
JP1ΔCT
B
Mock
PLCδPH
JP1ΔCT
KDa
Ca$_V$1.1
FLAG
250
100
50
20
C
PLCδPH
JP1ΔCT
5 pA/pF
10 ms
D
nC/μF
PLCδPH
JP1ΔCT
mV
E
Ca$_V$1.1
FLAG
Control
JP1ΔCT-FLAG
F
Control
JP1ΔCT-FLAG
Ca$_V$1.1-RyR
Ca$_V$1.1-RyR
PLA positive area per cell area (%)
G
Control
JP1ΔCT
Ca$_V$1.1-JP1
Ca$_V$1.1-JP2
RyR-JP1
RyR-JP2
PLA positive area per cell area (%)
H
Tetanus
ICE
Amplitude (ΔF/F$_0$)
1 s
50 s
Peak amplitude (ΔF/F$_0$)
Control
JP1ΔCT
I
IB:
Control
JP1ΔCT
Ca$_V$1.1
JP1ΔCT
JP1
JP2
IP: Ca$_V$1.1
Ca$_V$1.1-JP1 binding (AU)
Ca$_V$1.1-JP2 binding (AU)
J
Control
JP1ΔCT
Specific forces (mN/mm^2)
Stimulation frequency (Hz)

Fig. S1

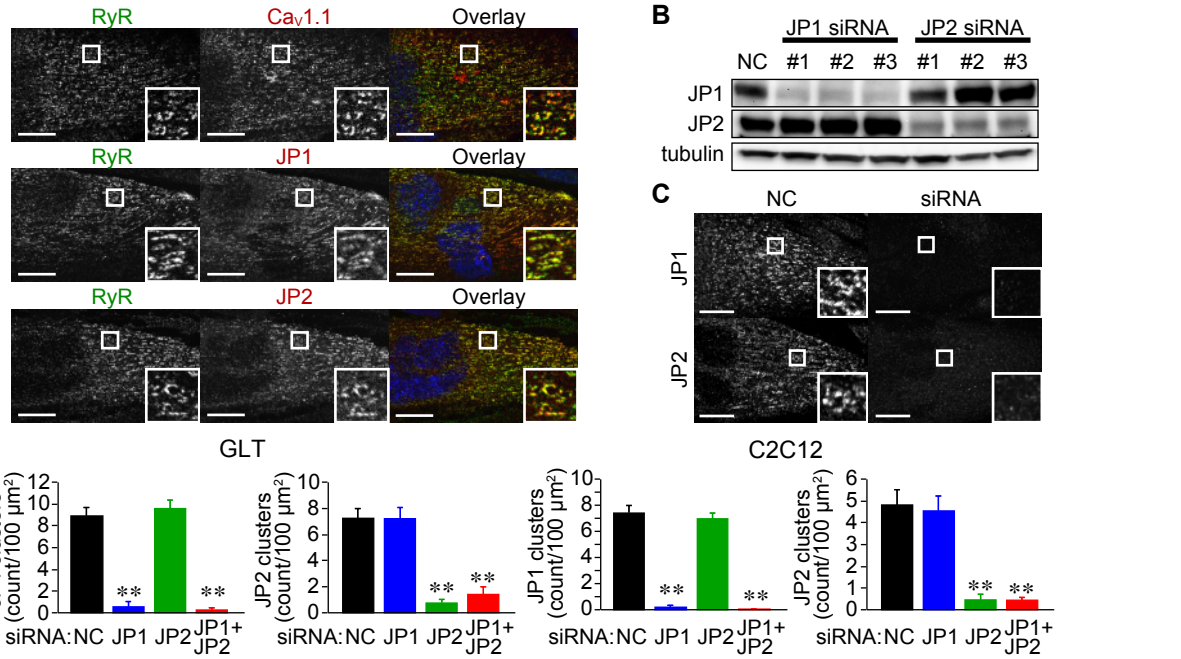
A
RyR
Cav1.1
Overlay
RyR
JP1
Overlay
RyR
JP2
Overlay
B
JP1 siRNA
JP2 siRNA
NC
#1
#2
#3
#1
#2
#3
JP1
JP2
tubulin
C
NC
siRNA
JP1
JP2
D
GLT
C2C12
JP1 clusters (count/100 μm²)
JP2 clusters (count/100 μm²)
siRNA: NC
JP1
JP2
JP1+ JP2
**

Fig. S2

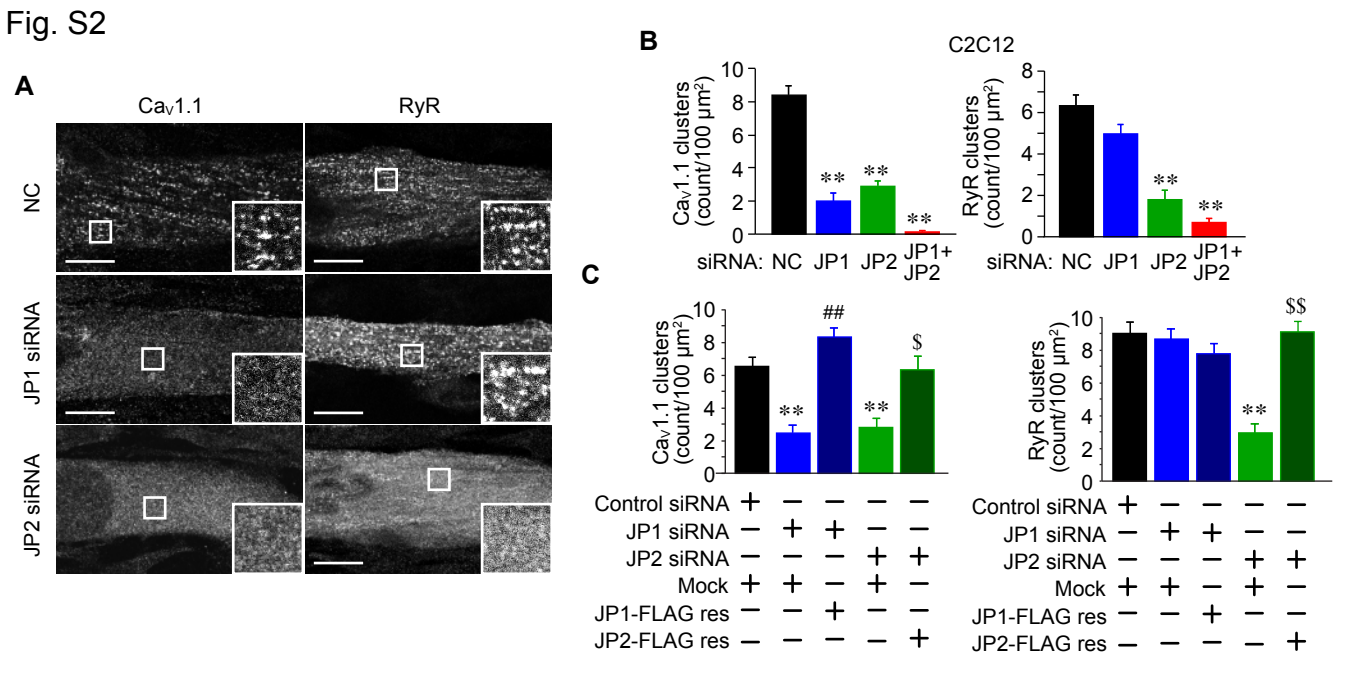
A
Cav1.1
RyR
NC
JP1 siRNA
JP2 siRNA
B
C2C12
Cav1.1 clusters (count/100 μm²)
RyR clusters (count/100 μm²)
siRNA: NC JP1 JP2 JP1+ JP2
C
Control siRNA
JP1 siRNA
JP2 siRNA
Mock
JP1-FLAG res
JP2-FLAG res

Fig. S3

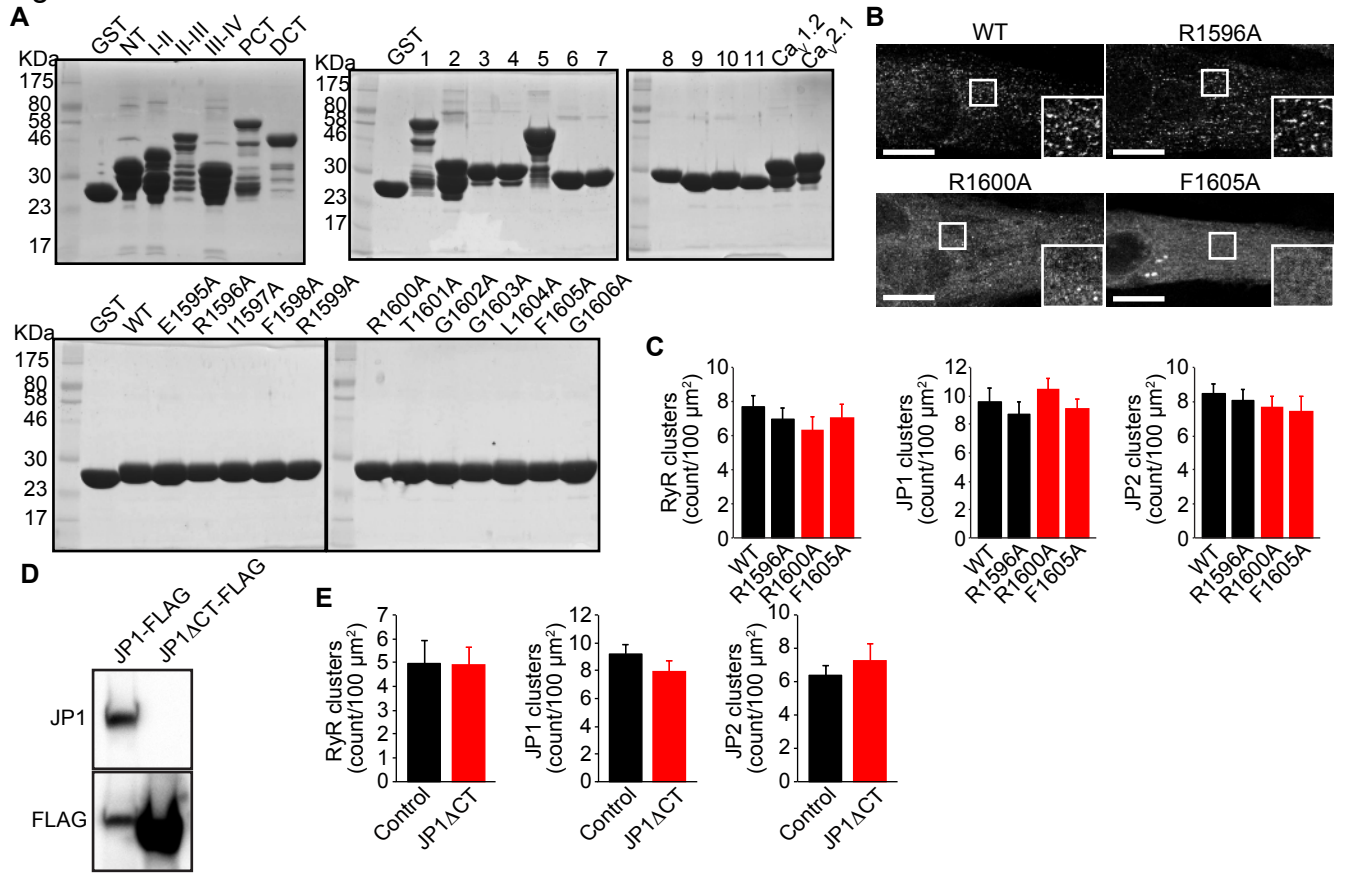
A
KDa
GST
NT
I-II
II-III
III-IV
PCT
DCT
175
80
58
46
30
23
17
GST
1
2
3
4
5
6
7
8
9
10
11
Cav1.2
Cav2.1
GST
WT
E1595A
R1596A
I1597A
F1598A
R1599A
R1600A
T1601A
G1602A
G1603A
L1604A
F1605A
G1606A
B
WT
R1596A
R1600A
F1605A
C
RyR clusters (count/100 μm²)
JP1 clusters (count/100 μm²)
JP2 clusters (count/100 μm²)
WT
R1596A
R1600A
F1605A
D
JP1-FLAG
JP1ΔCT-FLAG
JP1
FLAG
E
RyR clusters (count/100 μm²)
JP1 clusters (count/100 μm²)
JP2 clusters (count/100 μm²)
Control
JP1ΔCT

Fig. S4

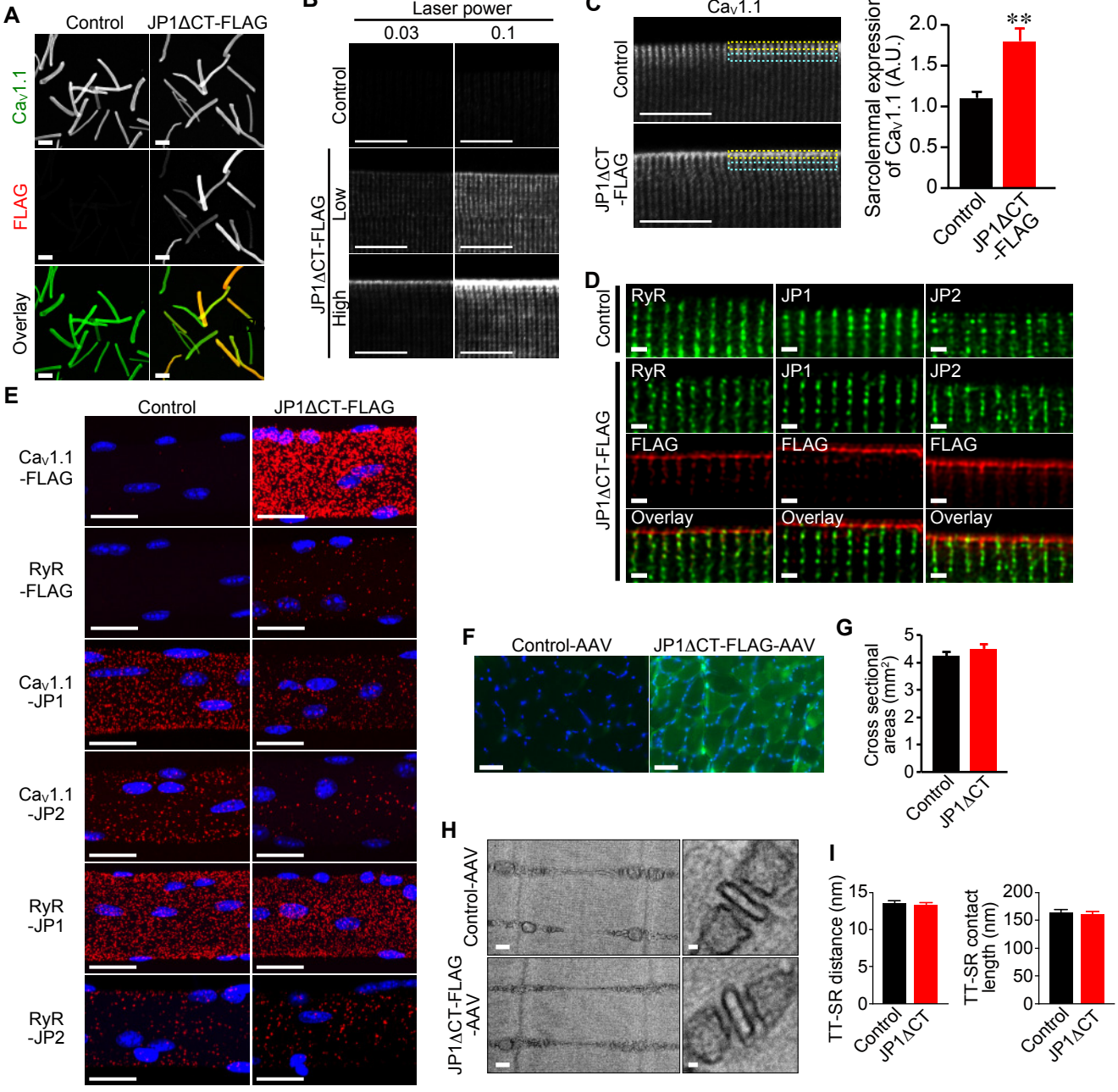
A
Control
JP1ΔCT-FLAG
CaV1.1
FLAG
Overlay
B
Laser power
0.03
0.1
Control
JP1ΔCT-FLAG
Low
High
C
CaV1.1
Control
JP1ΔCT -FLAG
Sarcolemmal expression of CaV1.1 (A.U.)
2.0
1.5
1.0
0.5
0
**
Control
JP1ΔCT -FLAG
D
Control
JP1ΔCT-FLAG
RyR
JP1
JP2
FLAG
Overlay
E
Control
JP1ΔCT-FLAG
CaV1.1 -FLAG
RyR -FLAG
CaV1.1 -JP1
CaV1.1 -JP2
RyR -JP1
RyR -JP2
F
Control-AAV
JP1ΔCT-FLAG-AAV
G
Cross sectional areas (mm2)
5
4
3
2
1
0
Control
JP1ΔCT
H
Control-AAV
JP1ΔCT-FLAG -AAV
I
TT-SR distance (nm)
15
10
5
0
Control
JP1ΔCT
TT-SR contact length (nm)
200
150
100
50
0
Control
JP1ΔCT